Influence of Blood Inertia on Vortex Enhancement in the Wake of Plaque Deposited Arteries

MUHAMMAD ANWAR SOLANGI*, AHSANULLAH BALOCH**, AND RAFIQUE AHMED MEMON***

RECEIVED ON 22.12.2009 ACCEPTED ON 08.06.2010

ABSTRACT

Flow of blood structure is presented in terms of stream line projections at different percentages of deposition against various Reynolds numbers. The impact of atherosclerosis is investigated on the vortex enhancement and intensity. The predicted results are computed in terms of stream function for quantifying the reattachment length and re-circulating flow rate of blood at various Reynolds numbers and different percentages of blockage. The results show that flow of blood is disturbs at the vicinity of blockage, especially in the down stream area that leads to the formation of vortexes. It is observed that the length of vortex increases along with the deposition levels as well as with increasing inertia .To solve the Navier-Stokes equations, together with the incompressibility constraints a semi-implicit time stepping procedure, namely Taylor-Galerkin/Pressure-correction finite element scheme has been employed.

Key Words: **Numerical Simulation, Atherosclerosis, Blood Flow, Capillaries, Newtonian Fluid.**

1. INTRODUCTION

Cardiovascular disease has been one of the most severe diseases for many decades, causing a large number of deaths worldwide each year, especially in developed countries. The presence of a partial occlusion in the human circulatory system may substantially alter the flow field and subsequently the flow rate of blood leading to severe incidences such as cardiac arrest and stroke. The role of hemodynamics in the arterial network and furthermore in the development of atherosclerosis formation has been under investigation for many years [1-5].

Arteriosclerosis is a common disease which severely influences human health. Early arteriosclerotic lesions are not randomly distributed throughout the arterial tree; they usually tend to form and grow at certain locations, such as the distal to abdominal aorta, coronary arteries, and carotid bifurcations [6]. It has been found that the initiation and localisation of arteriosclerosis is closely related to local hemodynamic factors (such as wall shear stress, etc.). Although there remains some uncertainty with regard to the exact hemodynamic factors responsible for the initiation of arteriosclerosis, it has been

* Assistant Professor, Department of Basic Sciences & Related Studies, Mehran University of Engineering & Technology, Jamshoro
** Professor, Department of Basic Sciences & Related Studies, Mehran University of Engineering & Technology, Jamshoro
*** Ph.D. Student, Centre of Advanced Studies in Pure & Applied Mathematics, Bahauddin Zakariya University, Multan.

demonstrated that the development of arteriosclerosis is strongly related to the characteristics of the blood flow in the arteries [7].

Flow of blood has been studied by many researchers and performed experimental, and numerical investigations on plaque deposited artery segment. The bending, blockage, bifurcation, etc of the arteries plays an important role for narrowing the blood vessels causing the disturbances in the flow field of blood [8]. Experimental work has been performed in rigid blockage arteries, showing that deposition of plaque change the local hemodynamics conditions due to the reduction in diameter of the blood vessels [9-10]. Pulsatile flow of blood in flexible deposition has been investigated [11]. Whilst numerical studies for axially symmetric plaque deposited arteries with the assumption of blood as incompressible Newtonian fluid has been discussed [12]. Furthermore,[13]have taken the non-Newtonian properties of blood into consideration, to predict the impact of irregular blockage in the artery segment.

To simulate the Navier-Stokes equations, together with the incompressibility constraints, a semi-implicit time stepping procedure, namely Taylor-Galerkin/pressure-correction finite element scheme has been used. The fundamental approach behind this technique is to derive highly accurate time-stepping scheme to compute transient as well as steady flow problems. Originally, this method was proposed by (Donea [14]) to solve the time dependent viscous flows in which the incompressible conditions treated implicitly.

This paper describes a computational method for simulating the flow of blood in arteries with applications in medical research and device design of cardiovascular physiology. This paper is structured as: In Section 2, complete problem is specified along with initial and boundary conditions, where as governing equations are addressed in Section 3. Numerical scheme is presented in section 4 and section 5, comprises the predicated results and discussions to investigate effects of blood inertia at different Reynolds numbers on various levels of deposition.

2. PROBLEM SPECIFICATION

The vessel segment having an axially symmetric deposition of plaque, in both axial and radial directions is considered increasing and is mathematically modelled as a rigid tube with a circular section. Let (r,z) be the coordinates where the z-axis is taken as axial direction along the axis of the artery in the flow of blood, while r is along the radial direction respectively. The deposition of plaque in artery is assumed in parabolic form with increasing length and percentage of blockage, is modelled using flowing equation:

$$r_n = r_0\left[1+\frac{k}{100}\frac{(a-Z_c)(b-Z_c)}{h^2}\right] \quad (1)$$

where r_n denotes the radius of the arterial segment in the blockage region, r_0 is the radial coordinates of the straight artery in the non-blockage region, h is the height of the deposition of plaque, k is the percentage of blockage of the artery, a and b denotes two points of the blockage region/length and Z_c is axial coordinates of the blockage region/length.

The geometry of the artery with boundary conditions is modelled as shown in the Fig. 1.

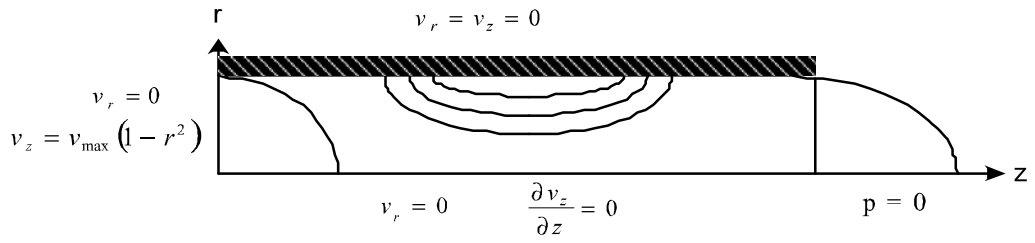

FIG. 1. ARTERY SEGMENT HAVING AN AXIALLY SYMMETRIC DEPOSITION OF PLAQUE

The computation region is 0<Z<70R, where the Z has been non-dimensionalised. The total artery length is taken as 70R and the length of upstream from deposition of plaque centre is taken as 15R for fully developed inlet boundary condition and 55R for downstream artery.

The initial and boundary conditions are necessary to be prescribed for completing the problem specification. For this, the initial conditions consist of specifying the value of v at the initial time; $\nu(z,) = \nu_o(z)$ subject to $\Delta.\nu_o=0$.

The boundary conditions are taken as essential condition, at the inlet of the artery; axial velocity is taken maximum defined by the function $\nu_z=\nu_{max}(1-R^2)$. In reality, walls of the arteries are not solid, here as initial study walls are assumed solid. Therefore no slip boundary conditions are imposed on the walls of the arteries. As on the assumption that blood flow is axi-symmetric, therefore, only the upper-half flow of blood in the plaque deposition artery region is simulated. Hence, at axis of symmetry vanishing normal velocity components are imposed along with both tangential tractions and tractions-free velocity components are tested. Radial velocity is taken zero, because there is no cross flow in r-direction. The inclusion of pressure often takes the form of a constant pressure upstream and downstream by the specification of p at a single point often as p=0 at the exit.

3. GOVERNING EQUATIONS

The Newtonian behaviour of blood flowing through large arteries can be mathematically modelled by the equation of continuity and the Navier-Stokes equations, in the absence of body force in the cylindrical polar coordinates frame of reference. These governing equations are given as under:

Equation of Continuity

$$\Delta.\nu = 0 \tag{2}$$

Navier-Stokes Equation

$$\rho\frac{\partial \boldsymbol{v}}{\partial t} = \mu\nabla^2\boldsymbol{v} - \rho\,\boldsymbol{v}.\nabla\boldsymbol{v} - \nabla p \tag{3}$$

Where ρ is the density of blood, ν is the velocity component, μ is the viscosity of blood, p is the isotropic pressure and (Δ and Δ^2) are the gradient and Laplacian operators respectively.

4. NUMERICAL SCHEME

For the numerical simulation the choice of numerical algorithm is based on its accuracy, stability, efficiency and convergence rate. Literature shows that in the explicit schemes, the convergence rate is slow and requires small time-steps, which leads to apply the alternative approaches of semi-implicit techniques [15-17]. Generally the implicit numerical schemes usually enhance the numerical stability but are also computationally more expensive. Therefore, here employing the semi-implicit scheme by introducing implicitness on viscous or diffusive components only using θ method and θ is taken as 0.5 due to Crank-Nicolson. The fully discrete semi-implicit system of equations is then as follows:

Stage-1(a):

$$\left[\frac{2}{\Delta t}M + \frac{1}{2\,\mathrm{Re}}S_{rr,j}\right](V_{r,j}{}^{n+\frac{1}{2}} - V_{r,j}{}^{n}) = \left[-\frac{1}{\mathrm{Re}}S_{rr}\,V_{r,j} - L_1^t P_k\right]^n - N(V)\,V_{r,j} \tag{4}$$

$$\left[\frac{2}{\Delta t}M + \frac{1}{2\,\mathrm{Re}}S_{zz,j}\right](V_{z,j}{}^{n+\frac{1}{2}} - V_{z,j}{}^{n}) = \left[-\frac{1}{\mathrm{Re}}S_{zz}\,V_{z,j} - L_2^t P_k\right]^n - N(V)\,V_{z,j} \tag{5}$$

Stage-1(b):

$$\left[\frac{1}{\Delta t}M + \frac{1}{2\,\mathrm{Re}}S_{rr}\right]\left(V_{r,j}{}^{*} - V_{r,j}{}^{n}\right) = \left[-\frac{1}{\mathrm{Re}}S_{rr}\,V_{r,j} - L_1^t P_k^n\right]^n - N(V)V_{r,j}^{n+\frac{1}{2}} \tag{6}$$

$$\left[\frac{1}{\Delta t}M + \frac{1}{2\,\mathrm{Re}}S_{zz}\right](V_{z,j}{}^{*} - V_{z,j}{}^{n}) = \left[-\frac{1}{\mathrm{Re}}S_{zz}\,V_{z,j} - L_2^t P_k^n\right]^n - N(V)\,V_{z,j}^{n+\frac{1}{2}} \tag{7}$$

Stage- 2:

$$K\left(Q^{n+1}\right) = -\frac{2}{\Delta t}\left(L_1\,V_{r,j} + L_2\,V_{z,j}\right) \tag{8}$$

Stage 3:

$$M\left(V_{r,j}^{n+1} - V_{r,j}^{*}\right) = \frac{\Delta t}{2} L_1^{t}\left(p^{n+1} - p^{n}\right) \quad (9)$$

$$M\left(V_{z,j}^{n+1} - V_{z,j}^{*}\right) = \frac{\Delta t}{2} L_2^{t}\left(p^{n+1} - p^{n}\right) \quad (10)$$

Where M is a consistent mass matrix, S is a momentum diffusion matrix, N(V) is a convection matrix, L is a pressure gradient matrix and K is stiffness matrix.

The system matrices are defined as:

$$M = \int_{\Omega} \Phi_i \Phi_j \, r \, d\Omega \quad (11)$$

$$L_1 = \int_{\Omega} \psi_i \frac{\partial \Phi_j}{\partial r} r \, d\Omega + \int_{\Omega} \psi_i \, \Phi_j \, d\Omega \quad (12)$$

$$L_2 = \int_{\Omega} \psi_i \frac{\partial \Phi_j}{\partial z} r \, d\Omega \quad (13)$$

$$L = \int_{\Omega} \psi_i \frac{\partial \Phi_j}{\partial z} r \, d\Omega \quad (14)$$

$$N(V) = \int_{\Omega} \Phi_i \left(\Phi_l \, V_l \frac{\partial \Phi_j}{\partial r} + \Phi_l \, V_l \frac{\partial \Phi_j}{\partial z} \right) r \, d\Omega \quad (15)$$

$$K_{ij} = \int_{\Omega} \frac{\partial \psi_i}{\partial r} \frac{\partial \psi_k}{\partial r} r \, d\Omega \quad (16)$$

$$S = \begin{bmatrix} S_{rr} & 0 \\ 0 & S_{zz} \end{bmatrix} \quad (17)$$

Where

$$S_{rr} = \int_{\Omega} \left(\frac{\partial \Phi_i}{\partial r} \frac{\partial \Phi_j}{\partial r} + \frac{\partial \Phi_i}{\partial z} \frac{\partial \Phi_j}{\partial z} + \frac{\Phi_i \Phi_j}{r^2} \right) r \, d\Omega \quad (18)$$

$$S_{zz} = \int_{\Omega} \left(\frac{\partial \Phi_i}{\partial r} \frac{\partial \Phi_j}{\partial r} + \frac{\partial \Phi_i}{\partial z} \frac{\partial \Phi_j}{\partial z} \right) r \, d\Omega \quad (19)$$

Where V^n_j is a nodal velocity vector at time t^n, V^*_j is an intermediate non-divergence-free velocity vector and V^{n+1}_j is a divergence-free velocity vector at time step t^{n+1}. Whilst P^n_k is a pressure Vector and $Q^{n+1}=-P^n_k$ is a pressure difference vector.

Stage one and three are governed by augmented mass-matrices and solved by a Jacobi iterative method, that necessitates using only a small fixed number of mass iterations typically, three or so. At stage two, Poisson equation matrix is symmetric and positive definite with a banded structure, for which it is appropriate to employ a direct Choliski method.

For the time marching procedure the pre-defined level of tolerance to which steady-state convergence is taken to be of the order of 10^{-6}.

5 RESULTS AND DISCUSSION

Flow of blood structure is presented in terms of streamline projections, at constant incremental values in the two regions, that is, a main core flow and recirculation of blood flow region. In the main flow region five contours are selected from $1x10^{-4}$ to $2.499x10^{-1}$ with equal increments of non-dimensional stream function value of $6.245x10^{-2}$. In the recirculating blood flow region four contours are selected at a constant increment $2.264x10^{-2}$ from $-7.938x10^{-2}$ to $-1.145x10^{-2}$. At artery wall, vanishing boundary conditions for stream function are fixed. Therefore, in recirculating region streamlines are negative. As the artery segment is very thin, therefore the behaviour of streamlines can not be visualized clearly. Hence aspect ratio has been increased five times.

5.1 Influence of Inertia on Vortex Enhancement

In Fig-2-4 (a-c) streamline projections for three different Reynolds numbers = 100, 200, and 300 at three levels of deposition (30, 50 and 70%) are presented, so that the effect of blood inertia at different Reynolds numbers on

various levels of deposition is to be investigated in terms of flow field. It is clear that significant vortex activity can be generated through blood inertia, producing embryo recirculation region to vortex enhancement, even at low Reynolds number. This flow phenomenon of vortex enhancement is observed that the length of recirculation region increases in the downstream as the Reynolds number and deposition of plaque increases.

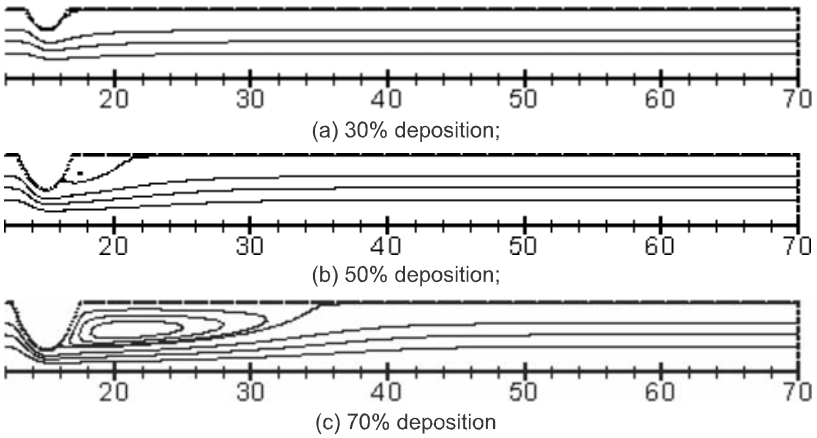

FIG. 2. STREAM-LINE PROJECTIONS AT REYNOLDS NUMBER RE=100 FOR DIFFERENT LEVELS OF DEPOSITION

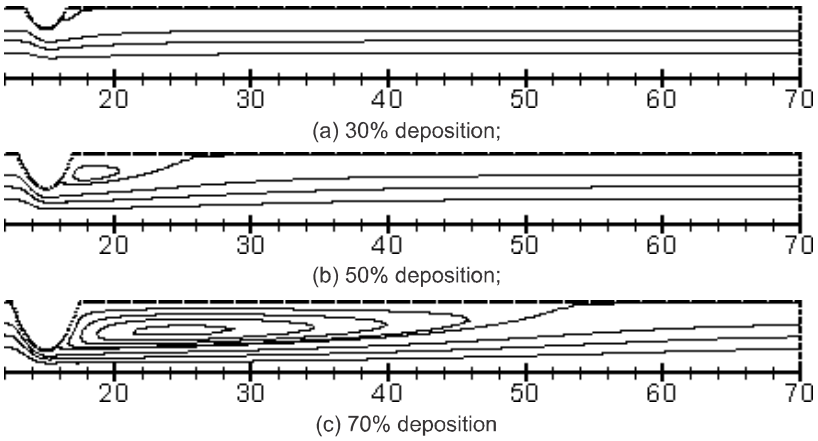

FIG. 3. STREAM-LINE PROJECTIONS AT REYNOLDS NUMBER RE=200 FOR DIFFERENT LEVELS OF DEPOSITION

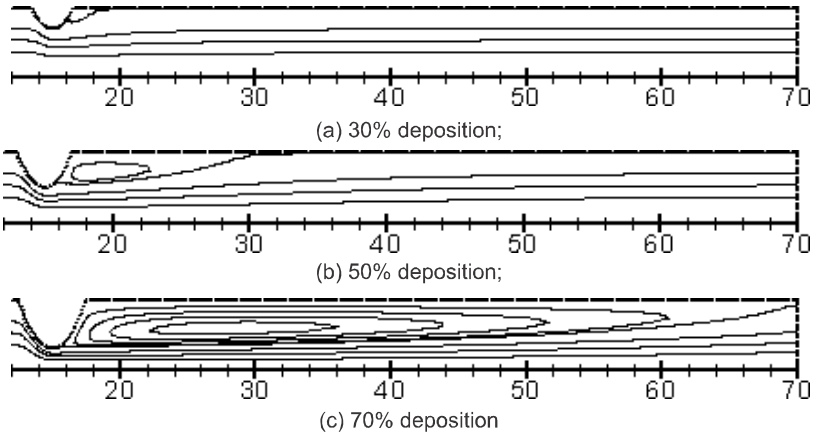

FIG. 4. STREAM-LINE PROJECTIONS AT REYNOLDS NUMBER RE=300 FOR DIFFERENT LEVELS OF DEPOSITION:

The streamline projections shows the marked effects on flow field at different levels of deposition, whereas at 30% deposition negligible vortex is formed and even for 50% deposition there is a small recirculation zone and for 70% deposition the recirculation zone is dominant in the flow field.

Reattachment length displayed in Table 1 is the axial distance from the centre of deposition to the point, where the recirculation ends. It is the region where adverse pressure gradient becomes negative and thus velocity becomes negative. The vortex length is computed in a down stream of the vessel segment having an axially symmetric deposition of plaque at two different locations of Z as:

$$L_v = \frac{Z_2 - Z_1}{2R} \tag{20}$$

Where R is the radius of the artery and Z_1 and Z_2 are two different locations in axial direction, one is taken at start of recirculation region in the vicinity of mid-plane of plaque deposition and second is taken far away end of recirculation, on the artery wall at downstream respectively. The values of Z_1 and Z_2 are computed through Regula- Falsi method utilizing vorticity and Z coordinates.

The computed vortex length against Reynolds numbers at various percentages of deposition of plaque at downstream is illustrated in Fig. 5. The behaviour clearly indicates linear growth of vortex length up to 60% of deposition of plaque, beyond 60% of blockage linear trend remains only at low Reynolds number. However, the length of vortex increases very high along high Reynolds number or high level of deposition or both.

TABLE 1. LENGTH OF VORTEX AGAINST REYNOLDS NUMBERS FOR DIFFERENT PERCENTAGES OF DEPOSITION

Re	Vortex Length					
	30%	40%	50%	60%	65%	70%
50	0.0	0.38	1.22	2.57	3.50	4.69
100	0.24	1.05	2.58	5.22	7.12	9.57
150	0.50	1.63	3.79	7.70	10.55	14.27
200	0.74	2.17	4.94	10.09	13.91	18.90
250	0.95	2.67	6.05	12.43	17.21	23.50
300	1.16	3.16	7.14	14.73	20.49	27.17

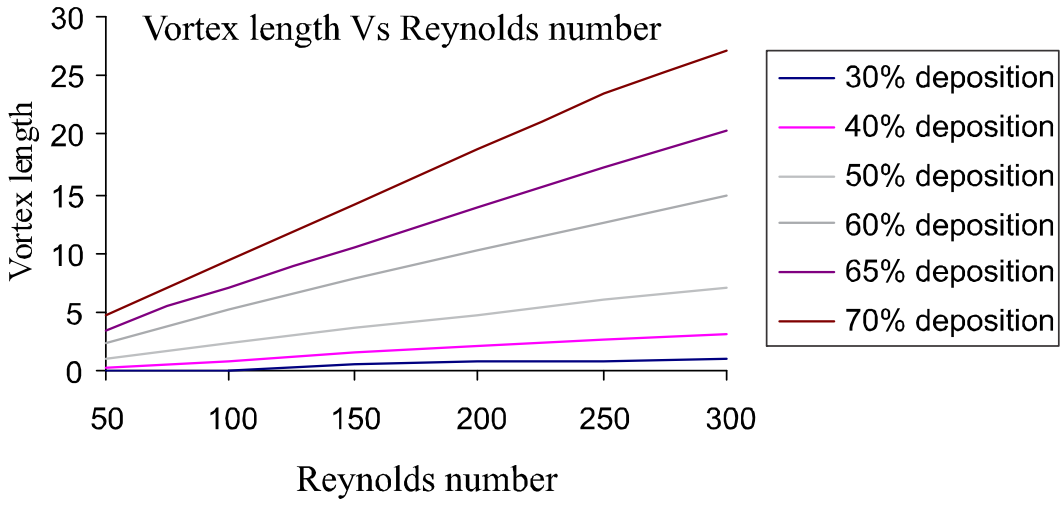

FIG. 5. VORTEX LENGTH AT DOWNSTREAM AGAINST REYNOLDS NUMBERS FOR DIFFERENT PERCENTAGES OF DEPOSITION

The computed vortex length against depositions of plaque at downstream for various Reynolds numbers is illustrated in Fig. 6. The behaviour of vortex length is observed second order polynomial for different percentages of deposition of plaque.

From Table 1, it is clear that at different plaque depositions with increasing Reynolds numbers the length of vortex increases. Further it is observed that the formation of vortex starts from 30% blockage at various Reynolds numbers and onwards plaque depositions, except 30% deposition at Reynolds number 50.

The empirical equations in terms of linear trend and the length of vortex for different percentages of deposition against various Reynolds numbers have been computed in the Table 2.

The empirical equations in terms of polynomial trend of second order have been computed for length of vortex verses different percentages of deposition against various Reynolds numbers displayed in the Table 3.

5.2 Influence of Inertia on Vortex Intensity

The vortex intensity (re-circulating flow rate (Q_v) is defined as the difference in stream function values from the periphery of the outer-most contour (Ψ_{peri}) of the vortex to the vortex centre (Ψ_c):

$$Q_v = \Psi_{peri} - \Psi_c \quad (21)$$

The intensity of vortices is monitored in terms of the ratio of the re-circulating flow rate to that in the core flow.

Streamline projections for three levels of deposition (30, 50 and 70%) at three different Reynolds numbers = 100,

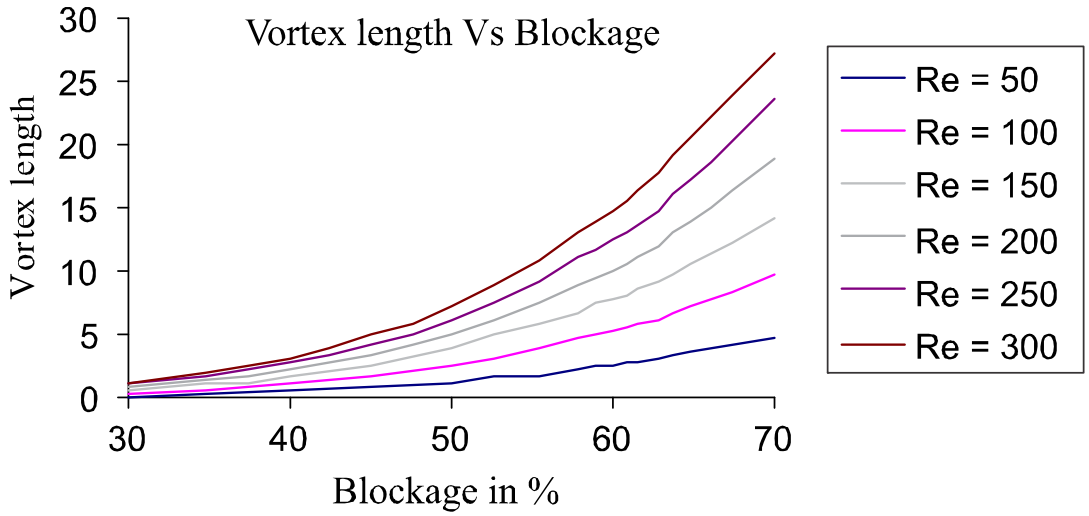

FIG. 6. VORTEX LENGTH AT DOWNSTREAM AGAINST BLOCKAGE FOR DIFFERENT REYNOLDS NUMBERS

TABLE 2. VORTEX LENGTH AT DOWNSTREAM AGAINST REYNOLDS NUMBERS FOR DIFFERENT PERCENTAGES OF DEPOSITION IN TERMS OF EQUATIONS

No.	Deposition	Equation
1.	30%	$L_v=4.7\times10^{-3}$ Re -0.2187
2.	40%	$L_v=1.1\times10^{-2}$ Re -0.0867
3.	50%	$L_v=2.35\times10^{-2}$ Re +0.1707
4.	60%	$L_v=4.85\times10^{-2}$ Re +0.308
5.	65%	$L_v=6.78\times10^{-2}$ Re +0.272
6	70%	$L_v=9.08\times10^{-2}$ Re +0.468

200, and 300 are presented, in Figs. 7-9(a-c) for investigating the effect of blood inertia on different levels of deposition at different Reynolds numbers in the flow field. It is observed that the intensity of blood increases with increasing deposition level or the Reynolds number.

The computed vortex intensity against Reynolds numbers for various percentages of deposition of plaque at downstream is presented in Table 4 and the behavior of vortex intensity verses Reynolds number is observed logarithmic, how ever, this trend terms to be nonlinear and reaches at plateu at very high Reynolds number, illustrated in Fig. 10. The computed vortex intensity against depositions of plaque at downstream for various Reynolds numbers is illustrated in Fig. 11. The behavior of vortex intensity is observed second order polynomial for different percentages of deposition of plaque.

TABLE 3. VORTEX LENGTH AT DOWNSTREAM AGAINST BLOCKAGE (B_k) FOR DIFFERENT REYNOLDS NUMBERS IN TERMS OF EQUATIONS

No.	Reynolds Number	Equation
1.	50	$L_v=2.8x10^{-3}\ (B_k)^2\ -1.691x10^{-1}\ (B_k)\ +2.5497$
2.	100	$L_v=5.8\ x10^{-3}\ (B_k)^2\ -3.563\ x10^{-1}\ (B_k)\ +5.7898$
3.	150	$L_v=9x10^{-3}\ (B_k)^2\ -5.655x10^{-1}\ (B_k)\ +9.551$
4.	200	$L_v=1.22x10^{-2}\ (B_k)^2\ -0.7511\ (B_k)\ +13.446$
5.	250	$L_v=1.54x10^{-2}\ (B_k)^2\ -1.0003\ (B_k)\ +17.391$
6.	300	$L_v=1.75x10^{-2}\ (B_k)^2\ -1.1131\ (B_k)\ +19.126$

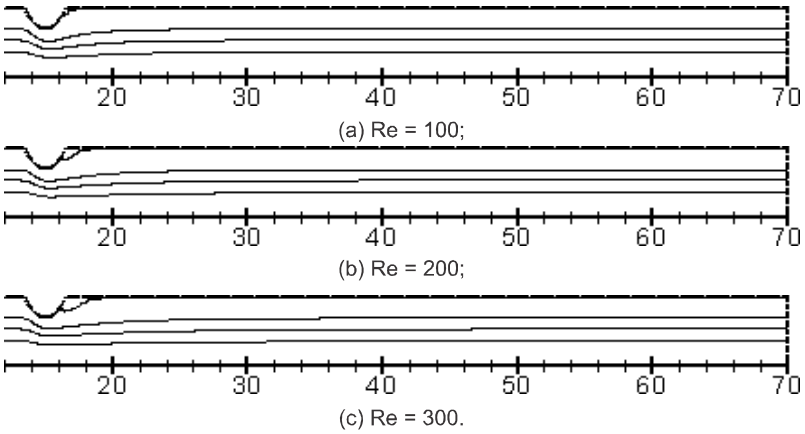

FIG. 7. STREAM-LINE PROJECTIONS FOR 30% LEVEL OF DEPOSITION AT VARIOUS REYNOLDS NUMBERS

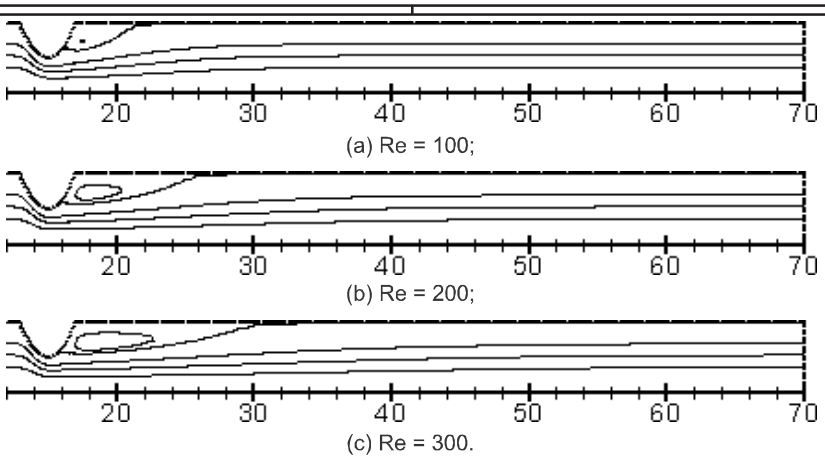

FIG. 8. STREAM- LINE PROJECTIONS FOR 50% LEVEL OF DEPOSITION AT VARIOUS REYNOLDS NUMBERS

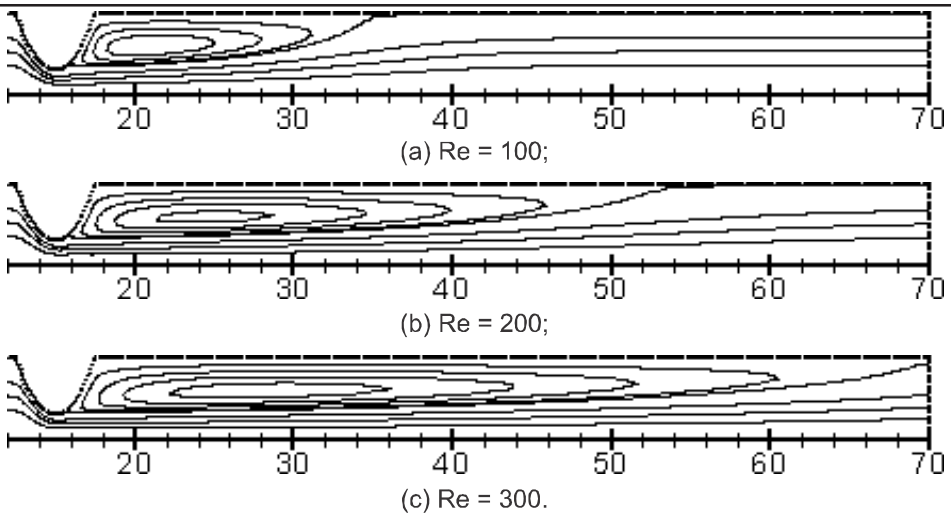

FIG. 9. STREAM- LINE PROJECTIONS FOR 70% LEVEL OF DEPOSITION AT VARIOUS REYNOLDS NUMBERS

TABLE 4. VORTEX INTENSITY AGAINST REYNOLDS NUMBERS FOR DIFFERENT PERCENTAGES OF DEPOSITION

Re	Vortex Length					
	30%	40%	50%	60%	65%	70%
50	0	0.000276	0.00495	0.020961	0.036105	0.060161
100	0.0001289	0.002301	0.011721	0.03237	0.049779	0.075573
150	0.0003922	0.004597	0.015603	0.03771	0.05616	0.08212
200	0.0008367	0.006223	0.018133	0.041065	0.060039	0.086019
250	0.0014652	0.007439	0.019979	0.043438	0.062733	0.089556
300	0.001939	0.008409	0.021417	0.045246	0.064749	0.090707

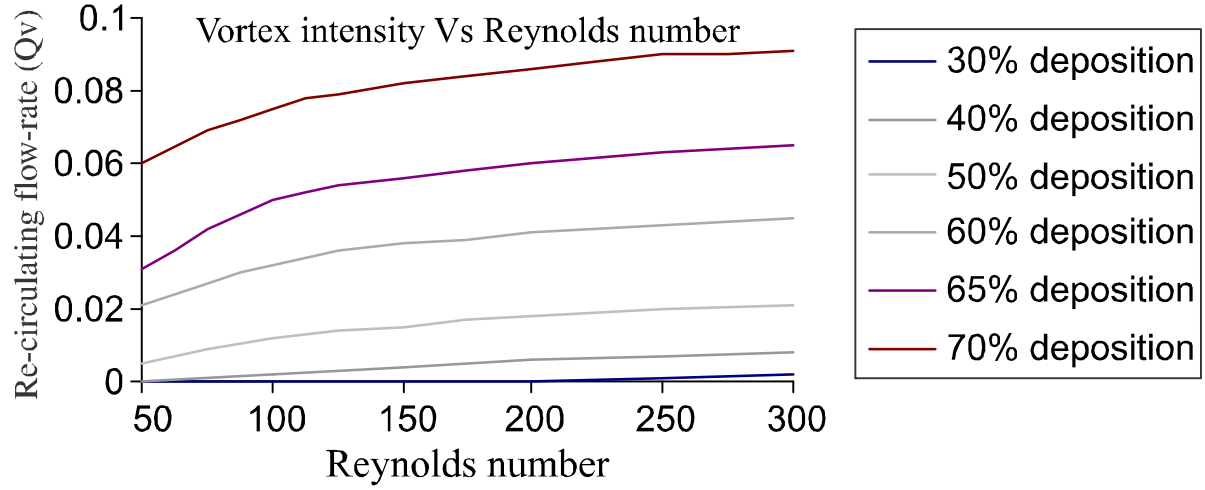

FIG. 10. VORTEX INTENSITY AT DOWNSTREAM AGAINST REYNOLDS NUMBERS FOR DIFFERENT PERCENTAGES OF DEPOSITION

The empirical equations in terms of logarithmic trend of vortex intensity for different percentages of deposition against various Reynolds numbers have been computed in the Table 5.

The empirical equations in terms of second order polynomial trend of vortex intensity against different levels of deposition for various Reynolds numbers have been presented in the Table 6.

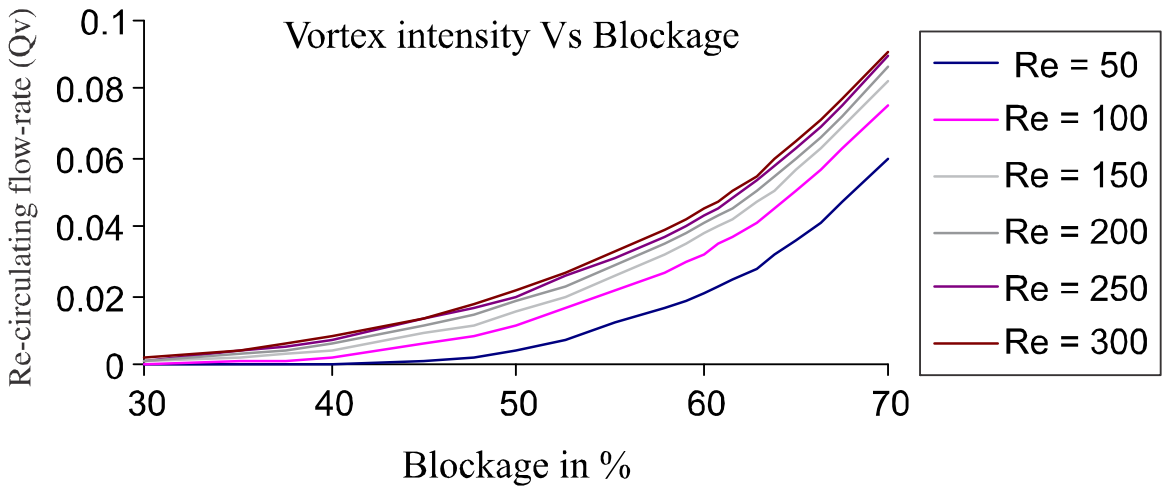

FIG. 11. VORTEX INTENSITY AT DOWNSTREAM AGAINST BLOCKAGE FOR DIFFERENT REYNOLDS NUMBERS

TABLE 5. VORTEX INTENSITY AT DOWNSTREAM AGAINST REYNOLDS NUMBERS FOR DIFFERENT PERCENTAGES OF DEPOSITION IN TERMS OF EQUATIONS

No.	Deposition	Equation
1.	30%	Q_v=0.001 ln (Re) -0.0044
2.	40%	Q_v=0.0047 ln (Re) -0.0185
3.	50%	Q_v=0.0092 ln (Re) -0.0309
4.	60%	Q_v=0.0135 ln (Re) -0.0309
5.	65%	Q_v=0.0185 ln (Re) -0.0385
6.	70%	Q_v=0.0171 ln (Re) -0.0052

TABLE 6. VORTEX INTENSITY AT DOWNSTREAM AGAINST BLOCKAGE (B_k) FOR DIFFERENT REYNOLDS NUMBERS IN TERMS OF EQUATIONS

No.	Reynolds Number	Equation
1.	50	$Q_v=6x10^{-5}\ (B_k)^2 -5x10^{-3}\ (B_k) +9.37x10^{-2}$
2.	100	$Q_v=7x10^{-5}\ (B_k)^2 -4.8x10^{-3}\ (B_k) +8.75\ x10^{-2}$
3.	150	$Q_v=6x10^{-5}\ (B_k)^2 -4.6x10^{-3}\ (B_k) +8.04\ x10^{-2}$
4.	200	$Q_v=6x10^{-5}\ (B_k)^2 -4.4x10^{-3}\ (B_k) +7.62\ x10^{-2}$
5.	250	$Q_v=6x10^{-5}\ (B_k)^2 -4.4x10^{-3}\ (B_k) +7.64\ x10^{-2}$
6.	300	$Q_v=6x10^{-5}\ (B_k)^2 -4.2x10^{-3}\ (B_k) +7.25\ x10^{-2}$

6. CONCLUSION

Flow of blood structure is observed in terms of Streamline projections and the effect of blood inertia at different Reynolds numbers on various levels of deposition has been investigated. It is observed that blood inertia generates significant vortex activity, producing from embryo recirculation region to vortex enhancement, even at low Reynolds number. This flow phenomenon of vortex enhancement is observed that the length of recirculation region increases in the downstream as the Reynolds number and deposition of plaque increases. The streamline projections shows the marked effects on flow field at different levels of deposition, whereas at 30% deposition negligible vortex is formed and even for 50% deposition there is a small recirculation zone and for 70% deposition the recirculation zone is dominant in the flow field.

ACKNOWLEDGEMENT

Authors greatly acknowledge with thanks to the Higher Education Commission, Pakistan, for financial support through project No. 20-217/R&D/2003/615 under National Research Programme for Universities.

REFERENCES

[1] Buchanan, J.R., Kleinstreuer, C., Hyun, S., and Truskey, G.A., "Hemodynamics Simulation and Identification of Susceptible Sites of Atherosclerotic", Journal of Biomechanics, Volume 36, pp.1185, 2003.

[2] Andersson, H.I., Halden, R., and Glomsaker, T., "Modeling Fluid Mechanics in Individual Human Carotid Arteries", Journal of Biomechanics, Volume 33, pp. 1257, 2000.

[3] Bertolotti, C., and Deplano, V., "Numerical Simulations of Unsteady Flows in a Stenosed Coronary Bypass Graft", Journal of Biomechanics, Volume 33, pp. 1011, 1995.

[4] Chandran, K.B., "Cardiovasucalr Biomechanics", New York University, 1992.

[5] Deplano,V., and Siouffi, M., "Numerical Study of Fluid Flow Through Double Bell-Shaped Constrictions in a Tube", Journal of Biomechanics, Volume 32, pp. 1081, 1999.

[6] Gnasso, A.l., "In Vivo Association Between Low Wall Shear Stress and Plaque in Subjects with Asymmetrical Caotid Atherosclerosis", Stroke, Volume 28, pp. 993, 1997.

[7] Guzman, R., Abe, K., and Zarins, C., "Flow-Induced Arterial Enlargement is Inhibited by Suppression of Nitric Oxide Synthase Activity in Vivo", Surgery, Volume 122, pp. 273-279, 1997.

[8] Lei, M., Kleinstreuer, C., and Truskey, G. A., "Numerical Investigations and Prediction of Atherogenic Sites in Branching Arteries", Journal of Biomechanics, Volume 117, pp. 350-357, 1995.

[9] Ahmed, S.A., "An Experimental Investigation of Plustile Flow Through a Smooth Constriction", Experimental Thermal and Fluid Science, Volume 17, pp. 309-318, 1998.

[10] Siouffi, M., Deplano, V., and Pelissier, R., "Experimental Analysis of Unsteady Flows Through a Stenosis", Journal of Biomechanics, Volume 31, pp. 11, 1998.

[11] Stegiopulos, N., Spiridon M., Pythoud, F., and Meister, J.J., "Numerical Study of Pulsating Flow Through a Tapered Artery with Stenosis", Journal of Biomechanics, Volume 29, pp.31, 1996.

[12] Long, Q., Xu, X.Y., Ramnarine, K.V., and Hoskins, P., "Numerical Investigation of Physiologically Realistic Pulsatile Flow Through Arterial Stenosis", Journal of Biomechanics, Volume 34, pp. 1229, 2001.

[13] Tu, C., and Deville, M., "Numerical Analysis of Flow Through a Severely Stenotic Carotid Artery Bifurcation", Journal of Biomechanics, Volume 29, pp. 899, 1996.

[14] Donea, J., "A Taylor-Galerkin Method for Convective Transport Problems", International Journal of Numerical Method Engineering, Volume 20, pp. 101-119, 1984.

[15] Hawken, D.M., Tamaddon, Townsend, P., and Webster, M.F., "A Taylor-Galerkin Based Algorithm for Viscous Incompressible Flow", International Journal of Numerical Method Engineering, Volume 10, pp. 327-351, 1990.

[16] Carew, E.O.A., Townsend, P., and Webster, M.F., "On a Discontinuity Capturing Technique for Oldroyd-B Fluids", Journal of Non-Newtonian Fluid Mechanics, Volume 51 pp. 231, 1994.

[17] Baloch, A., Townsend, P., and Webster, M.F., "On the Highly Elastic Flows," Journal of Non-Newtonian Fluid Mechanics, Volume 75, pp.139-166, 1998.